A comparative study of different reliability methods for high dimensional stochastic problems related to earth dam stability analyses

X. Guo, D. Dias, C. Carvajal, L. Peyras, Pierre Breul

A comparative study of different reliability methods for high dimensional stochastic problems related to earth dam stability analyses

Xiangfeng Guo[1], Daniel Dias[1*], Claudio Carvajal[2], Laurent Peyras[2], Pierre Breul[3]

*1 Univ. Grenoble Alpes, CNRS, Grenoble INP**, 3SR, F-38000 Grenoble, France*

2 Irstea, RECOVER, F-13182 Aix-en-Provence, France

3 Univ. Clermont Auvergne, Institut Pascal, CNRS, F-63000 Clermont-Ferrand, France

*Corresponding author: daniel.dias@univ-grenoble-alpes.fr

**Institute of Engineering Univ. Grenoble Alpes

Abstract

This article presents a probabilistic stability analysis of an existing earth dam including uncertainty quantification of soil properties and a reliability analysis of the dam sliding stability. The analyses are conducted by exploiting the available field measurements, and then by performing the Monte Carlo Simulation (MCS). Random fields and random variables approaches are both used to model the soil variabilities. Two left-and-right-bounded distributions, beta and truncated normal, are considered for the input random variables in the reliability analysis, and the influence of the horizontal autocorrelation distance on the failure probability is investigated.

A comparative study of different reliability methods is also carried out by comparing with the results of the MCS. The considered reliability methods are: the Subset Simulation (SS), the Moment Method (MM), the Sparse Polynomial Chaos Expansion in combination with the Global Sensitivity Analysis (SPCE/GSA) and the Sparse Polynomial Chaos Expansion in combination with the Sliced Inverse Regression (SPCE/SIR). The comparative study shows that all these methods can give accurate results in term of the dam failure probability with small errors. It is also found that the most accurate method is the SPCE/GSA and the most efficient method is the SS.

Keywords: Earth Dam; Dam Factor of Safety; Reliability analysis; Random fields; Monte Carlo Simulations; Polynomial chaos expansions.

1 Introduction

Various uncertainties of soil properties (inherent spatial variability and measurement error) exist in earth dam engineering. Accounting for these uncertainties with specific methods and understanding their effects are of great value for dam design and safety assessment. In the literature, some studies related to probabilistic stability analyses of earth dams can be found [1–5]. However, most of the previous works simulated the uncertainties of soil properties by hypothetical or statistical considerations [1–4]. Another limitation of these existed studies is that soil spatial variabilities were generally ignored, such as in [1,3,4]. Additionally, only one reliability analysis result (reliability index or failure probability) was provided and no information about the distribution or the statistical moments for the factor of safety (FoS) was available in these studies [1–5].

This paper is dedicated to address the problems mentioned above by presenting a comprehensive reliability analysis of an earth dam. It includes quantification of soil properties, soil variability modelling from real field data, uncertainties quantification and failure probability estimation. The reliability analysis is based on the sliding stability analyses of the dam under steady state flow conditions. The uncertainties of three soil properties (dry density (γ_d), effective cohesion (C') and effective friction angle (ϕ')) are considered and simulated by random fields or random variables. The selected soil properties are the most relevant for a slope stability analysis (as showed in [5,6]) and they are sufficient for a probabilistic study under the present design scenario (with a steady state flow condition). An advantage of the studied dam is that it was well documented and there are a large number of measurements available. More importantly, the γ_d measurements are geo-localized during the embankment compaction, which allows a data geostatistical analysis and leads to a representation

of γ_d by random fields. The random fields of ϕ' can then be obtained by transforming the ones of γ_d using a physical relation (Caquot's relation as the works of [5]) and the C' is simulated by means of random variables. The propagation of these uncertainties is quantified by performing a classical MCS in combination with a mechanical model based on the limit equilibrium method which focuses on computing the dam FoS.

The second objective of the paper is to investigate the performance of four reliability methods. Considering these methods, the results are compared with the ones of MCS. Since small values of autocorrelation distance are obtained for the considered dam by analyzing the measurements, a large number of random variables (around 2000) is needed to represent accurately the random fields of γ_d. The present study becomes thus a very high dimensional stochastic problem. Therefore, the comparison study is focused on evaluating the performance of different reliability methods for very high dimensional stochastic problems. Few studies exist for the comparison of different reliability methods in real engineering problems and no study has been done for the stochastic problems with more than 1000 random variables in the geotechnical field. The selected four reliability methods to be assessed are explained as follows.

For a reliability analysis, the MCS is always considered as a standard reference to test other methods [7,8]. However, it suffers from a very low computational efficiency. Based on the MCS, two advanced sampling methods (Importance Sampling (IS) [7] and Subset Simulation (SS) [9]) were proposed to reduce the variance of the MCS estimator with a limited number of deterministic model calls. The SS can be used in a reliability analysis with both random variables approach and random fields approach as shown in [10], whereas the IS is not applicable for some cases with random fields if the involved random variables have no physical meaning. Another sampling-based technique is the Point Estimate Method (PEM) [11] which uses specific samplings to

86　　　estimate first moments of a system response and then to approximate reliability index

87　　　by the estimated moments. Alternatively, the first moments can also be determined by

88　　　performing an MCS until the convergence is reached. Furthermore, the First-Order

89　　　Reliability Method (FORM) and the Second-Order Reliability Method (SORM) are

90　　　also commonly used in the field of reliability [3,12]. They are usually employed in

91　　　combination with the Response Surface Method (RSM). The aim is to seek a so-called

92　　　design point by solving a constrained problem. Unfortunately, the FORM, SORM and

93　　　RSM are not able to handle too many random variables [13]. During the last decades,

94　　　meta-modelling techniques have received much attention in the reliability analysis

95　　　due to their efficiency and accuracy [14]. This technique allows constructing a

96　　　surrogate model (a.k.a. meta-model) to an original mechanical model. The constructed

97　　　meta-model is usually expressed in an analytical form. The computational burden is

98　　　thus quasi-negligible, which enables an MCS with respect to the meta-model. There

99　　　are several mathematical tools available to reach the goal of a meta-modelling, such

100　　as Artificial Neural Networks (ANN) [15,16], Kriging model [17–19] and Polynomial

101　　Chaos Expansions (PCE) [20,21]. In the context of high dimensional stochastic

102　　problems, some dimension reduction techniques were introduced and combined with

103　　the meta-modelling to improve its performance, such as the SPCE/GSA [22] and the

104　　SPCE/SIR [23] which were proposed in recent years. They use respectively the GSA

105　　and the SIR to reduce the number of the involved random variables at first stage, and

106　　then to construct an accurate SPCE meta-model based on the reduced dimension. In

107　　summary, the selected reliability methods for the comparative study in the article are

108　　thus: a variance reduced MCS (the SS), an MCS-based moment method (the MM),

109　　and two meta-modelling methods for high dimensional stochastic problems (the

110　　SPCE/GSA and the SPCE/SIR).

111

112　　The studied dam was investigated in a probabilistic framework by Guo et al. in [24].

113　　The authors studied the dam reliability by using the SPCE with the field data. The soil

114   variabilities of C', ϕ' and γ_d were simulated by means of random variables. Two

115   deterministic models were developed in [24] for evaluating the dam FoS. The present

116   study is dedicated to extend the studies in [24] by conducting a variogram analysis on

117   the geo-localised γ_d measurements to consider the soil spatial variabilities, and to

118   compare different reliability methods in related to the considered dam reliability. The

119   main objectives of the article are to present a thorough probabilistic stability analysis

120   of an earth dam, and to conduct a comparative study on the performance of different

121   reliability methods in a context of high dimensional stochastic problems. The

122   presented procedure and obtained results could help designers to better understand

123   reliability analyses of earth dams using real data, and to choose more specifically

124   reliability methods for future problems.

125

2 Random fields and Reliability analysis methods

This section aims at presenting all the reliability analysis tools used in the article. It includes the method for generating random fields, the variogram analysis and the selected reliability methods.

2.1 Simulation of random fields by the Karhunen–Loève expansion (K-L)

In this study, the K-L expansion method is adopted to simulate random fields. Let us consider a stationary Gaussian random field $H(x, \xi)$ in a bounded domain Ω. Following the principles of the K-L expansion, $H(x, \xi)$ can be expressed as [25]:

$$H(x, \xi) = \mu + \sigma \sum_{i=1}^{\infty} \sqrt{\lambda_i} \theta_i(x) \xi_i \approx \mu + \sigma \sum_{i=1}^{S} \sqrt{\lambda_i} \theta_i(x) \xi_i \qquad (1)$$

where x represents the coordinates of an arbitrary point in Ω, μ and σ are respectively the mean value and the standard deviation of the random field, ξ is a vector of standard uncorrelated random variable, λ_i and θ_i are respectively the eigenvalues and the eigenfunctions of the autocovariance functions of the random field, and S is the size of the series expansion for the truncated form. An autocovariance function is defined as the product of the variance and the autocorrelation function which gives a correlation value between two arbitrary points (x, y) and (x', y') in Ω. In this study, an exponential autocorrelation function is used [8].

The value of S depends on the desired accuracy, the autocorrelation distance (L_x, L_y) and the dimension of the random field. It can be determined by evaluating the error estimation of the truncated series expansion. The error estimate based on the variance of the truncated error for a K-L expansion with S terms is given by [26]:

$$\varepsilon = \frac{1}{\Omega} \int_{\Omega} \left[1 - \sum_{i=1}^{S} \lambda_i \theta_i^2(x) \right] d\Omega \qquad (2)$$

149 In order to obtain a sufficient accuracy in terms of the variance error for random
150 fields, Li and Der Kiureghian [27] recommended that the stochastic grid size of a
151 random field can be set as 0.2 times the autocorrelation distance. For the cases of non-
152 Gaussian random fields, it can be achieved by an isoprobabilistic transformation once
153 a Gaussian random field is obtained using the K-L expansion [28,29].

154 **2.2 Variograms**

155 A variogram is a function which provides a description of how data are correlated.
156 The first step of a variogram analysis is to construct an experimental variogram which
157 describes the correlation between any two values of the observation data separated by
158 a distance h. The experimental semivariogram γ^* is defined as [25]:

159

$$\gamma^*(h) = \frac{1}{2N_h} \sum_h \left(g_i - g_j\right)^2 \tag{3}$$

160 where g_i and g_j represent all the possible pairs of samples which are separated with a
161 distance of h, and N_h is the number of the pairs of g_i and g_j. This calculation should
162 be repeated for as many different values of h as the observation data will support.
163 Then a mathematical model is applied to the experimental semivariogram in order to
164 represent an autocorrelation structure over the whole study area and to estimate
165 autocorrelation distances. One of the most common variogram models is the
166 exponential model, which is used in this study and whose equation is [25]:

167

$$\gamma(h) = C\left[1 - e^{-(3h/a)}\right] \tag{4}$$

168 The parameter a represents the range of the variogram (also called autocorrelation
169 distance), and C is the sill value at which the variogram levels off. Figure 1 shows the
170 characteristics of a variogram analysis.
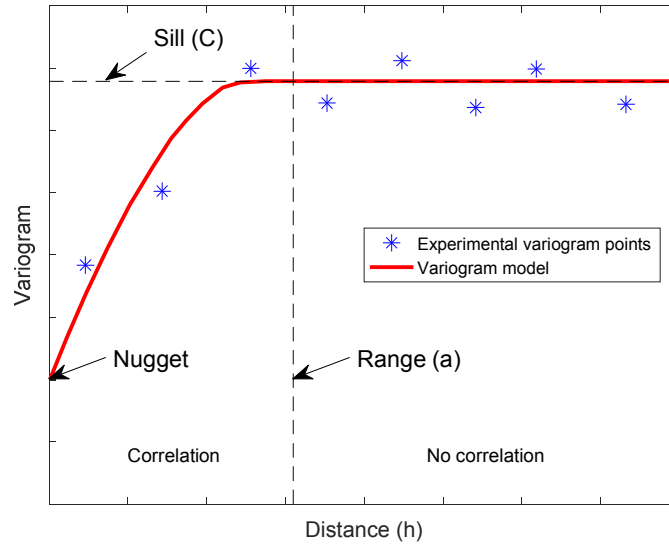
Figure 1. Characteristics of a variogram analysis

2.3 Presentation of the reliability methods used in the study

2.3.1 Monte Carlo Simulation (MCS): the reference method for the study

The MCS method has been widely employed in reliability analyses [30]. For an MCS

with N_{MCS} model runs, the failure probability is given as:

$$Pf = \frac{1}{N_{MCS}} * \sum_{j=1}^{N_{MCS}} I \qquad (I = 1 \; if \; G < 0; \; I = 0 \; else) \qquad (5)$$

where I is an index of failure and G presents a performance function. The number of

N_{MCS} should be large enough in order to obtain an accurate failure probability. The

coefficient of variation (CoV) of Pf for a MCS can be calculated by [26]:

$$CoV_{Pf} = \sqrt{(1 - Pf)/(N_{MCS} * Pf)} * 100\% \qquad (6)$$

Although this method suffers from low computational efficiency, it often serves as a

standard reference to test other reliability methods because of its versatility and

robustness. In this article, the reliability analysis of the studied dam is performed by

8

185 the MCS and the obtained results are used to evaluate the accuracy and the efficiency

186 of the selected reliability methods which are presented in next sub-sections.

2.3.2 Subset simulation (SS)

188 In order to tackle the problem of using the MCS especially for low failure probability

189 cases, the SS was developed by [9]. The principle is to decompose a failure event E

190 into a sequence of intermediate events $[F_1, F_2, ..., F_m]$ with larger probabilities of

191 occurrence. The target failure probability is written as [31]:

192

$$Pf = P(E) = P(F_1) \prod_{i=2}^{m} P(F_i|F_{i-1}) \tag{7}$$

193 where $P(F_i|F_{i-1})$ is the conditional failure probability of the event $F_i|F_{i-1}$. A key

194 element of successfully using the SS is the generation of the conditional samples in

195 each intermediate event. This is achieved by using the modified Metroplis-Hasting

196 algorithm (MMH) in this article.

2.3.3 Moment method approximation (MM)

198 The MM was introduced by [32] for structural reliability analyses. A well-known MM

199 is the second-moment approximation (SM). It assumes that a system response follows

200 a normal distribution and uses the first two moments to estimate the reliability index.

201 In the present study, a fourth-moment approximation (FM) is also used to estimate the

202 dam failure probability since it can give more accurate results compared to the SM as

203 reported in [33]. The formulas of the two adopted MM methods (SM and FM) are

204 given as follows [32]:

205

$$\beta_{SM} = \frac{\mu_G}{\sigma_G}; \quad Pf_{SM} = \Phi(-\beta_{SM}) \tag{8}$$

$$\beta_{FM} = \frac{3(\alpha_{4G} - 1)\beta_{SM} + \alpha_{3G}(\beta_{SM}^2 - 1)}{\sqrt{(9\alpha_{4G} - 5\alpha_{3G}^2 - 9)(\alpha_{4G} - 1)}}; \quad Pf_{FM} = \Phi(-\beta_{FM}) \tag{9}$$

206

207 where (β_{SM}, Pf_{SM}) and (β_{FM}, Pf_{FM}) are respectively the (reliability index, failure

208 probability) estimated by the SM and FM, μ_G, $\sigma_G{}^2$, α_{3G} and α_{4G} are the first four

209 statistical moments of the performance function, and $\Phi(\cdot)$ represents the cumulative

210 distribution function (CDF) of a standard normal variable. The values of the required

211 statistical moments are determined by an MCS in this study. The deterministic model

212 is repeatedly run for different sets of input parameters generated from a specific PDF,

213 until all the desired moments are converged.

214 **2.3.4 Spares polynomial chaos expansion/Global sensitivity analysis (SPCE/GSA)**

215 The SPCE/GSA was proposed by Sudret (2008) [34] and improved by Al-Bittar et al.

216 [22] for high dimensional stochastic problems. The SPCE presents a suitable sparse

217 basis of the PCE. The sparse basis can be built by a stepwise regression algorithm as

218 described in [21,35,36]. By using the SPCE, A model response can be expanded as

219 [36]:

220

$$Y \cong \sum_{\alpha \in \mathbb{N}^M} k_\alpha \Psi_\alpha(\xi) \tag{10}$$

221 where $\xi = \{\xi_1, \xi_2, \dots, \xi_M\}$ are independent random variables, $\Psi_\alpha(\xi)$ are

222 multivariate polynomials, k_α are unknown coefficients to be computed and $\alpha =$

223 $\{\alpha_1, \dots, \alpha_M\}$ is a multidimensional index. In this paper, the hyperbolic truncation

224 scheme proposed in [21] is used to truncate the series expansion and the unknown

225 coefficients k_α are computed by using the least-regression method [36].

226

227 Concerning the GSA, it allows quantifying contributions of an input variable to the

228 response variance of a physical model [34]. Sudret (2008) [34] introduced an

229 analytical way to compute the Sobol index (a sensitivity index) by post-processing the

230 SPCE coefficients. The Sobol index of one variable can be calculated as:

231

$$S(\xi_i) = \frac{\sum_{\boldsymbol{\alpha} \in A_{\xi_i}} (k_j)^2 E[(\Psi_{\boldsymbol{\alpha}})^2]}{\sum_{\boldsymbol{\alpha} \in A} (k_j)^2 E[(\Psi_{\boldsymbol{\alpha}})^2]} \tag{11}$$

where k_j are PCE coefficients, A is a truncation set, A_{ξ_i} is a subset of A in which the multivariate polynomials $\Psi_{\boldsymbol{\alpha}}$ are only functions of the random variable ξ_i (i.e., they only contain the variable ξ_i), and $E[(\Psi_{\boldsymbol{\alpha}})^2]$ is the expectation of $(\Psi_{\boldsymbol{\alpha}})^2$.

As a summary, the SPCE/GSA implementation for a reliability analysis consists of 3 steps:

1. Select significant input variables by performing a GSA based on a 2-order SPCE. It should be noted that the SPCE order has almost no influence on the Sobol index, so an SPCE with the order 2 can accurately provide contributions of each input variable to system response variabilities [22,34],
2. Construct a meta-model using a high-order SPCE with the selected variables (effective dimension),
3. Perform an MCS using the obtained meta-model to compute the system response PDF and the failure probability.

2.3.5 Spare polynomial chaos expansion/Sliced inverse regression (SPCE/SIR)

The SPCE/SIR was proposed by [23]. The principle remains the same to the SPCE/GSA which lies on a dimension reduction before construction of an accurate SPCE meta-model. The SPCE/GSA utilizes the GSA to reduce the number of the involved random variables, while it is achieved by another technique named SIR in the SPCE/SIR. This approach is based on the principle that a few linear combinations of original input variables could capture essential information of a model response [37]. It aims to find an effective dimension reduction (EDR) space by considering an inverse regression relation which regresses input variables against model responses. The algorithm presented in [23] is adopted in this study to find the EDR. By performing this algorithm, a new input vector can be obtained which is a linear combination of original input variables, and the dimension is reduced. Once the new input vector is determined, an accurate SPCE model can be constructed and then the failure probability can be estimated with an MCS.

3 Study case presentation: soil properties available and variability modelling

This section focuses firstly on presenting the studied earth dam and describing the available field data. Then, the statistical parameters of the three soil properties ($C', \phi' \ and \ \gamma_d$) required for generating random fields or random variables are determined using the field data.

3.1 Presentation of the studied dam

Figure 2 presents the main cross section of the considered dam. It is a 170 m long and 23.8 m high earth-filled dam located in the west of France. It closes a valley covered with alluvial deposits and can retain a reservoir of about 5 hm^3. The normal and maximal reservoir water level is respectively 20 and 21.6 m. In the downstream part, two filter drains were installed for the purpose of lowering the phreatic surface [38]. In the foundation, a waterproof grout curtain was realized with a depth of 15 m.
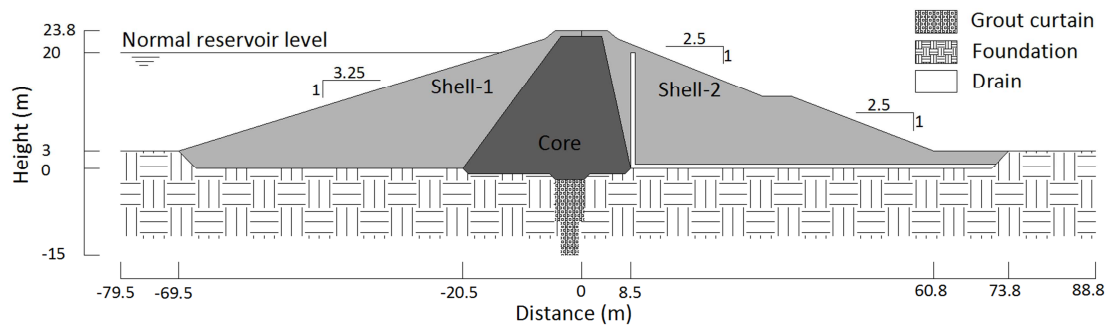
Figure 2. Main cross section of the studied dam

As presented in Figure 2, the dam is formed by three different zones including a core and two backfill zones in respectively the upstream and downstream part of the core. These three zones are respectively named as Core, Shell-1 and Shell-2 in this article. The materials constituting the dam were collected from the vicinity of the dam site. Two different types of soils can be identified in the valley. The first type is gravelly sands resulting from alteration of shales on the slopes and uplands which dominate the

12

282 valley. This material is used for the construction of the Shell zone. The second soil

283 type, sandy silts, can be found on the bottom of the valley and on the slopes. It was

284 used for the construction of the Core zone. The foundation is composed of altered

285 schists whose superficial layers have been purged. Its location is very close to the

286 Shell zone according to the site investigation and granulometric analyses.

3.2 The available field data

288 Different data are available on the studied earth dam in several phases: design studies,

289 construction controls and structure monitoring. This article presents only the field data

290 which are relevant to the stability analysis of dams: dry density measurements

291 collected during the construction and the results of the triaxial tests performed in

292 laboratories. The former is directly related to the γ_d and the latter allows estimating

293 C' and ϕ'.

3.2.1 Embankment compaction

295 During the construction, the dry density and the soil water content after compaction

296 were monitored in-situ using a gammadensimeter. This leads to a large number of γ_d

297 data. An advantage of these data is that they were collected following a grid

298 monitoring system. This makes it possible to localize the measurements in space

299 (along three axes). The grid system consists of 10 profiles in the longitudinal direction

300 (Y axis) and 13 profiles in the transversal direction (X axis). Such a grid system

301 allows determining the location of the measurements on an X-Y plan and the

302 knowledge of the construction layer gives the elevation of the measurements along the

303 Z axis. In total, the number of effective geo-localized γ_d measurements is 381 for the

304 Core zone, 248 for the Shell-1 zone and 272 for the Shell-2 zone.

3.2.2 Triaxial shear tests

306 The shear strength parameters were determined by triaxial shear tests. For a long-term

307 stability analysis of earth dams, the effective cohesion and friction angle are required.

308 Concerning these parameters, totally 8 consolidated-undrained triaxial shear tests with

309   pore water pressure measurement are available. Among the 8 tests, 5 tests are for the

310   Shell zone and the other 3 for the Core zone. By plotting the Mohr circles of the

311   effective stress at failure, the values of C' and $tan\phi'$ can be estimated using the

312   Coulomb line (approximately tangent to all the circles). Using this method, the results

313   of each test can be exploited to compute the values of C' and ϕ'. According to the 8

314   available tests, the average of C' is estimated to be equal to 9.4 kPa for the Shell zone

315   and to 10 kPa for the Core zone. For ϕ', a value of 34.2$^\mathrm{o}$ was obtained for the Shell

316   zone and of 34.3$^\mathrm{o}$ for the Core zone. It can be found that the shear strength parameters

317   for long term of the two soils are very close to each other. In fact, the two materials

318   are relatively similar as they derive from the schists alteration composing the bedrock.

319   The considered dam is actually a pseudo-zoned earth dam.

320   **3.3 Variability modelling of the soil properties**

321   In the present study, soil variability modelling consists of two steps. Firstly, an

322   appropriate distribution type is assumed and then the relating distribution parameters

323   are determined by fitting the measurements to the assumed distribution. Secondly,

324   autocorrelation structures are estimated through a variogram analysis based on the

325   geo-localized measurements. It is noted that the first step is directly related to the

326   works in [24]. Therefore, only a brief description of the first step is given in the

327   following parts.

328   **3.3.1 First step: Distribution type and relating parameters**

329   Two distribution types (beta and truncated normal distribution) are adopted as a

330   candidate, in this article, to describe the measured data of C', ϕ' and γ_d. The reason

331   of choosing the two distribution types is that they can avoid unreasonable values by

332   considering a physical range of soil properties. By fitting the measurements with the

333   beta or truncated normal distribution, the corresponding soil parameter can be

334   described as a random variable. The best fitted parameters are estimated using the

335   maximum likelihood estimation method, and the bounded values are determined
336   according to the soil type and the reference values recommend in [39,40].

337

338   The procedure of the first step mentioned above can be easily applied to the
339   measurements of γ_d since many data exist for this soil property in each zone of the
340   dam. However, the number of the available triaxial tests is only 8 and it does not
341   allow a meaningful statistical estimation of the distribution parameters for C' and ϕ'.
342   In order to address this problem, [5] introduced a method which can generate a large
343   number of artificial data for C' and ϕ' with limited triaxial test results. This method is
344   also adopted in the works of [24] to determine the distribution parameters with the
345   beta or truncated normal distribution for C' and ϕ' of the studied dam. With this
346   method, the distribution parameters for all the three soil properties (C', ϕ' and γ_d) can
347   be obtained. Table 1 gives a summary of the distribution parameters for each zone. As
348   an illustration, Figure 3 and Figure 4 present respectively the histogram and the two
349   fitted CDF curves for the γ_d measurements in the Core zone, and for the generated C'
350   in the Shell zone. The method introduced by [5] for determining the distribution
351   parameters of C' and ϕ' is based on a linear regression performed on the top of the
352   Mohr circles. This method assumes that the intermediate parameters (the y-intercept
353   and the slope of the Kf line) which are used for estimating the values of C' and ϕ',
354   are two uncorrelated normal variables. Therefore, no correlation is considered
355   between the shear strength parameters in this paper. According to previous works [41]
356   on slope reliability analyses, ignoring the correlation between C' and ϕ' which is
357   usually negative [42], leads to conservative estimates of failure probabilities.
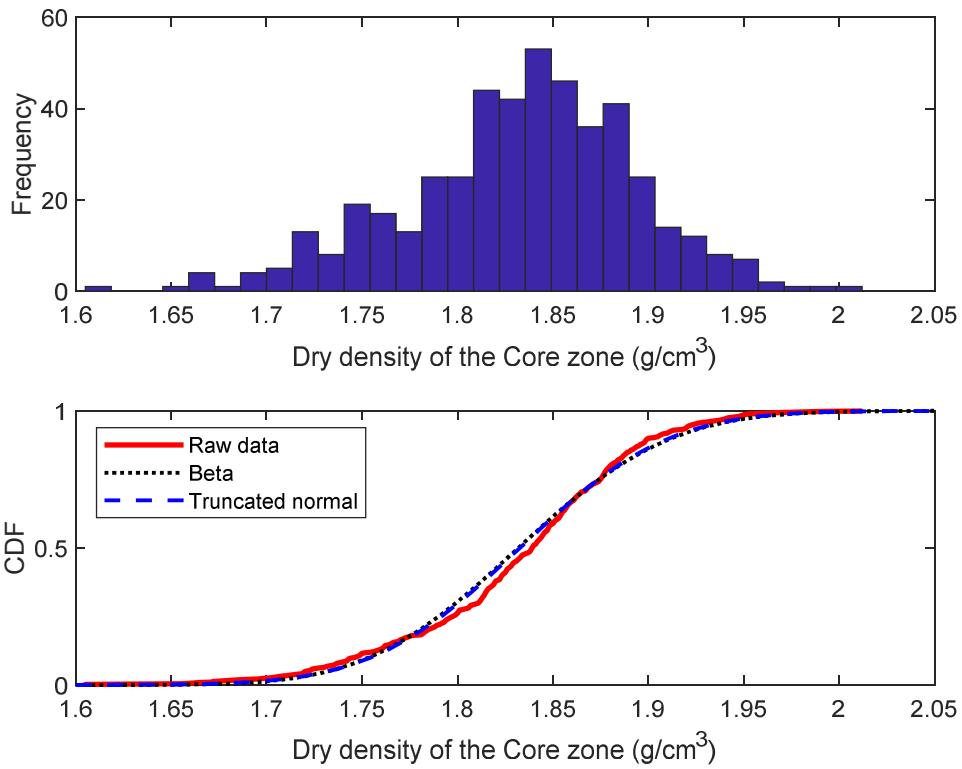
358

359   **Figure 3. Histogram and fitted CDF for the γ_d measurements in the Core zone**

360
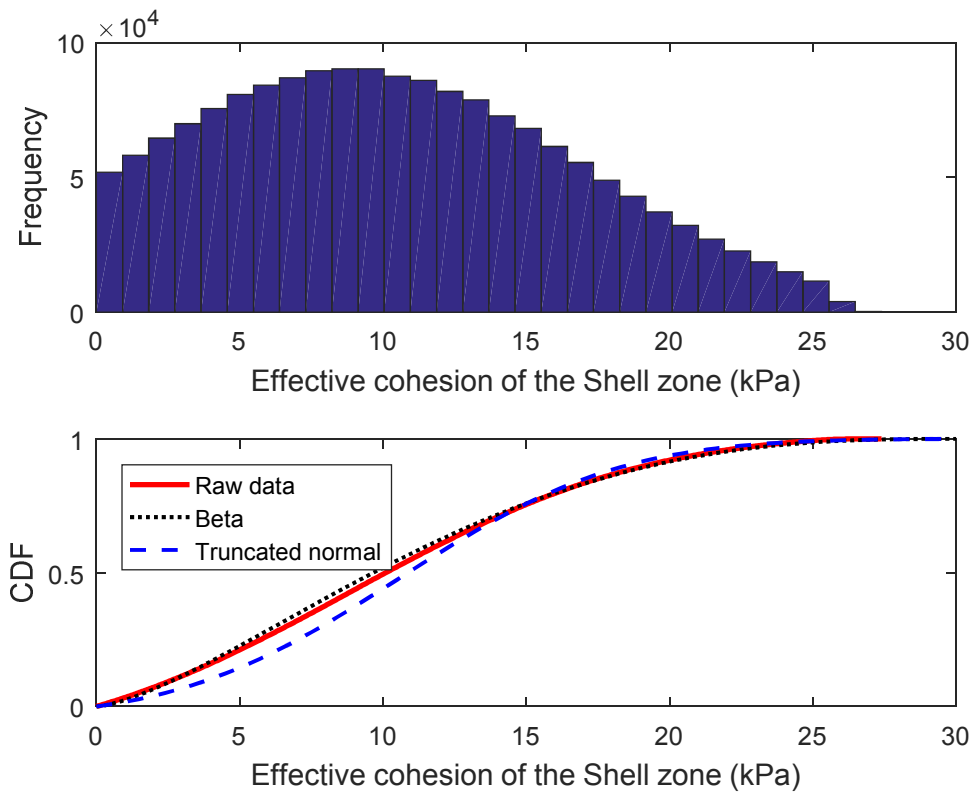
Figure 4. Histogram and CDF of the generated C' in the Shell zone

362 **Table 1. Distribution parameters of the soil properties**

Zones	Soil property	Beta		Truncated normal		Extreme values	
		a^1	b^1	Mean	CoV^2(%)	Min	Max
Shell-1	γ_d (g/cm^3)	15.7	18.0	1.99	3.21	1.63	2.40
	C' (kPa)	1.48	2.78	10.55	57.63	0	30
	ϕ' (^{o})	28.71	29.61	34.85	3.72	25	45
Core	γ_d (g/cm^3)	22.4	27.5	1.83	3.33	1.44	2.32
	C' (kPa)	4.07	5.22	13.23	34.21	0	30
	ϕ' (^{o})	231.16	192.28	34.11	2.48	15	50
Shell-2	γ_d (g/cm^3)	26.7	22.2	2.05	2.65	1.63	2.40
	C' (kPa)	1.48	2.78	10.55	57.63	0	30
	ϕ' (^{o})	28.71	29.61	34.85	3.72	25	45

363 Note: [1]Beta distribution parameters; [2]Coefficient of variation

3.3.2 Second step: Autocorrelation structure

365 The second step aims at determining the autocorrelation structure of the simulated soil
366 property for each dam zone. The method [5] adopted for generating values of C' and
367 ϕ' cannot provide the location information. Therefore, only the autocorrelation
368 structure of γ_d is estimated. It could be realized by a variogram analysis on the geo-
369 localized γ_d measurements. Taking the Shell-2 zone as an example, an experimental
370 semivariogram is firstly obtained by applying Eq. (3) to all the γ_d measurements of
371 this zone. Then, the autocorrelation distances can be estimated by fitting a
372 mathematical model (exponential one in this paper) to the experimental
373 semivariogram. Figure 5 shows the experimental semivariogram together with the
374 fitted exponential model for both horizontal and vertical directions. It can be observed
375 that the variance between two measurements increases with the increase of its
376 separation distance. The variance roughly reaches a constant value after the distance
377 beyond 5-7m for the horizontal directions. For the vertical direction, it converges

378   when the distance is bigger than 1.5m (lower value than for the horizontal direction).

379   The black points in Figure 5 represent the points which reach 95% of the sill value. It

380   is considered that the abscissa of these points is the autocorrelation distance. For the

381   cases in Figure 5, the horizontal and vertical distances are respectively 4.9 m and

382   1.9 m. It indicates that the soil is less homogeneous in the vertical direction than in the

383   horizontal direction. This finding is consistent with the observations of [42,43]. By

384   repeating the same procedure to the γ_d measurements in the other two zones Core and

385   Shell-1, all the necessary autocorrelation distances are obtained and presented in

386   Table 2.

387

388   Table 2 indicates that a considerable homogeneity can be found in the Shell-1 zone,

389   while the γ_d in the Shell-2 and Core zones are more spatially variable. This difference

390   can be explained by the better selection of the material composing the upstream zone

391   and the greater attention which has given to its construction. The nugget effect

392   corresponds to about a half of the variance for the upstream shoulder and to a slightly

393   lower fraction for the downstream shoulder and the core. The nugget effect can be

394   attributed to the mixture of the materials during their excavation from the borrow pits.

395   In our case, it is considered as a short dimension structure whose scale is less than the

396   sampling step.
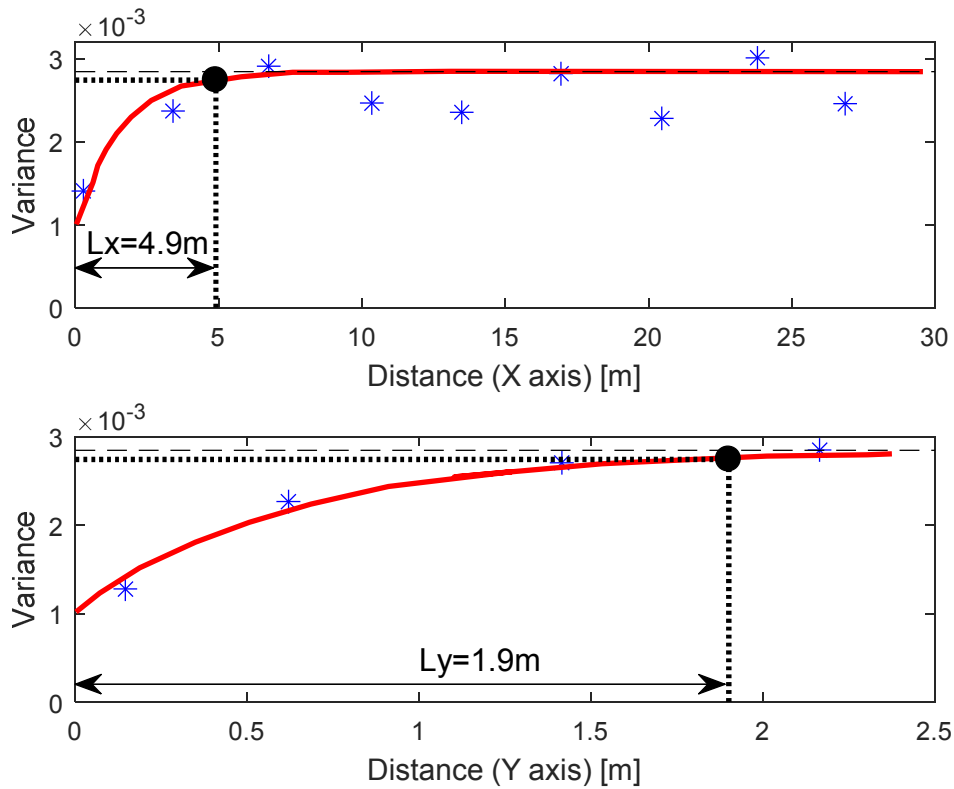
Figure 5. Variogram analysis for the γ_d measurements in the Shell-2 zone

Table 2. Results of the geostatistical analysis for the γ_d measuremetns

Zones	Autocorrelation distance (m)		Nugget effect
	Horizontal (L_x)	Vertical (L_y)	
Shell-1	78.1 m	7.8 m	1.6×10^{-3}
Core	13.0 m	1.5 m	8.6×10^{-4}
Shell-2	4.9 m	1.9 m	1.0×10^{-3}

As presented in section 2.1, a K-L expansion should be truncated to a limited number of series terms S for practical applications. The value of S can be determined by evaluating the error defined by Eq. (2) with a prescribed accuracy. This error depends on the autocorrelation distances and size of a random field. For an accuracy between 10% and 9%, the S is estimated to be equal to 30, 368 and 1710 for respectively the Shell-1, Core and Shell-2 zones (considering their site dimension and the relating

19

407 autocorrelation distances presented in Table 2). Therefore, it needs 1710 random

408 variables to represent accurately a random field of γ_d in the Shell-2 zone. Such small

409 values of the L_x and L_y in the Shell-2 zone lead to the present study become a very

410 high dimensional stochastic problem.

411 **3.4 Seismic loading condition**

412 A pseudo-static acceleration is considered in this study in order to take into account

413 seismic loading conditions. The value of the acceleration is set equal to 2.4 m.s^{-2}. It is

414 determined according to the location of the considered dam with respect to the seismic

415 zones in France and the category of the dam [44]. The seismic acceleration used in the

416 calculation is considered to be related to a return period of 5000 years. This means

417 that the failure probability directly obtained under such a pseudo-static acceleration

418 should be multiplied by 1/5000 to consider the seismic occurrence probability. The

419 two types of failure probability are respectively noted as Pf_{direct} and Pf_{con} in the

420 study.

4 Presentation of the deterministic models

422 Two deterministic models were developed in [24] for computing the dam FoS. The

423 first one is a numerical model based on the strength reduction method, and the second

424 one is an analytical model based on the limit equilibrium theory. The latter is

425 employed in this article to perform the deterministic calculations in the reliability

426 analyses since it can give similar FoS values compared to the numerical model but

427 with a lower computational time. Such an advantage is very significant and important

428 for a reliability analysis which needs usually a large number of calls to a deterministic

429 model. Concerning the numerical model, it was developed for providing the pore

430 water pressure distribution inside the dam and validating the analytical model.

431

432   This section aims at presenting the two models briefly. In the end, a comparison study

433   between the two models is conducted in order to validate the analytical model in the

434   context of random fields.

435   **4.1 The numerical model**

436   The numerical model in [24] was created using Flac2D which is a two-dimensional

437   explicit finite difference program [45]. The boundary conditions used in this model

438   are the following ones: the displacements are blocked following the horizontal and

439   vertical axis on the base of the model; the horizontal displacements are blocked on the

440   lateral edges of the model. Figure 6 presents a mesh used for the following

441   calculations. The mesh includes around 18000 4-node quadrilateral plane elements.

442   The selected number of the elements was determined by a mesh refinement study

443   [24]. The created model allows calculating the pore water pressure distribution inside

444   the dam by applying a hydrostatic head in the upstream. The dam FoS is computed

445   based upon the strength reduction method [6].
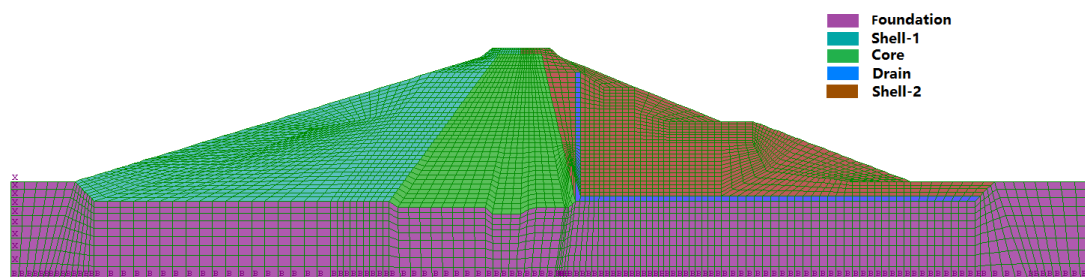
446

447   **Figure 6. The numerical model mesh of the studied dam**

448   **4.2 The analytical model**

449   The analytical model proposed in [24] is based on the limit equilibrium theory in

450   combination with a genetic algorithm (GA) [46]. The principle is to generate a

451   number of trial slip surfaces as an initial population at first, and then to search the

452   minimum FoS value by simulating natural process along generations including

453   reproduction, crossover, mutation and survivors' selection. The FoS of a given slip

454   surface is computed by using the procedure of Zhu et al. [23] which is based on the

455 Morgenstern Price method, and the slip surface generation method described in [24] is

456 adopted which allows generating non-circular slip surfaces. It is also noted that the

457 pore water pressures at the base of each slice are determined using the ones obtained

458 by the numerical model. For more details about the model, readers are referred to

459 [24].

460 **4.3 Validation of the analytical model**

461 It was shown in [24] that the analytical model is able to give similar FoS values in a

462 deterministic calculation and similar reliability results in a probabilistic calculation

463 compared to the numerical model. However, the comparison and validation studies

464 conducted in [24] are only related to the cases of random variables. The performance

465 of the analytical model in the context of random fields is thus still unknown. In order

466 to address this issue, a comparison study is carried out and presented in this section.

467 The idea is to generate N_{com} random fields for ϕ' and γ_d, and N_{com} random variables

468 for C'. For each set of input parameters, the two deterministic models are both

469 performed. The obtained FoS values are then compared with each other to evaluate

470 the accuracy of the analytical model. The numerical model is adopted as a reference to

471 assess the performance of the analytical model for the following reasons: 1) no

472 assumptions are needed concerning the failure surface, 2) no assumptions on inter-

473 slice side forces are needed, since there is no concept of slices, and 3) no optimization

474 procedure is needed since the minimum FoS and the critical slip surface are obtained

475 automatically.

476

477 In total 150 sets of input parameters are considered in the comparison study. Each set

478 of input parameters is obtained randomly and is composed of three random fields of

479 γ_d, three random fields of ϕ' and two random variables of C'. The other soil

480 parameters, except C', ϕ' and γ_d, required for the numerical model are taken from the

481 values given in [24]. The values of the GA parameters in the analytical model are the

482   same to the ones in [24]. As an illustration, a realization of three random fields of γ_d

483   are mapped to the numerical model and presented in Figure 7. Using the Caquot's

484   relation, three random fields of ϕ' are also obtained and shown in Figure 8.

485

486   Figure 9 presents a direct comparison of the FoS values computed with the two

487   models for the 150 different parameter sets. It is shown that the results are close to the

488   unit line and relative errors are smaller or around 5%. These observations indicate that

489   the analytical model is able to estimate an accurate FoS value for the studied dam

490   considering random fields. Therefore, the analytical model is validated and can be

491   used for deterministic calculations for the following reliability analyses.

492
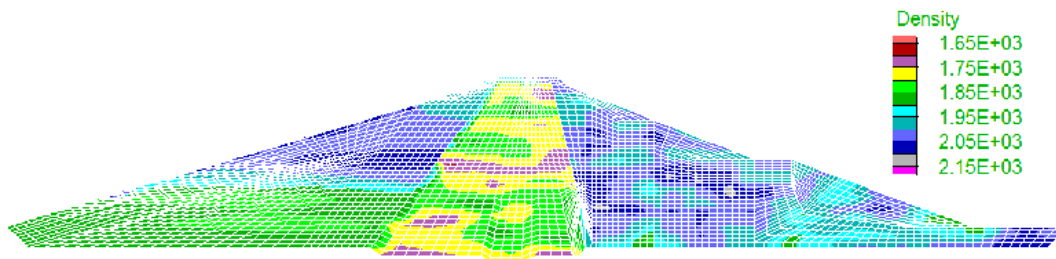
493   **Figure 7. Example of a realization of three random fields of γ_d**

494
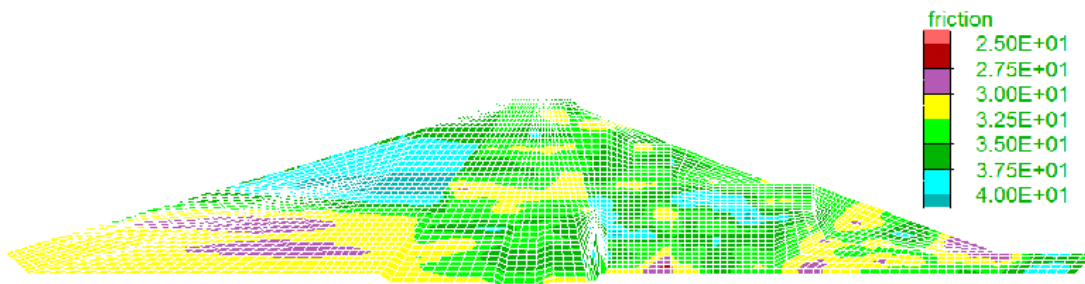
495   **Figure 8. Example of a realization of three random fields of ϕ'**
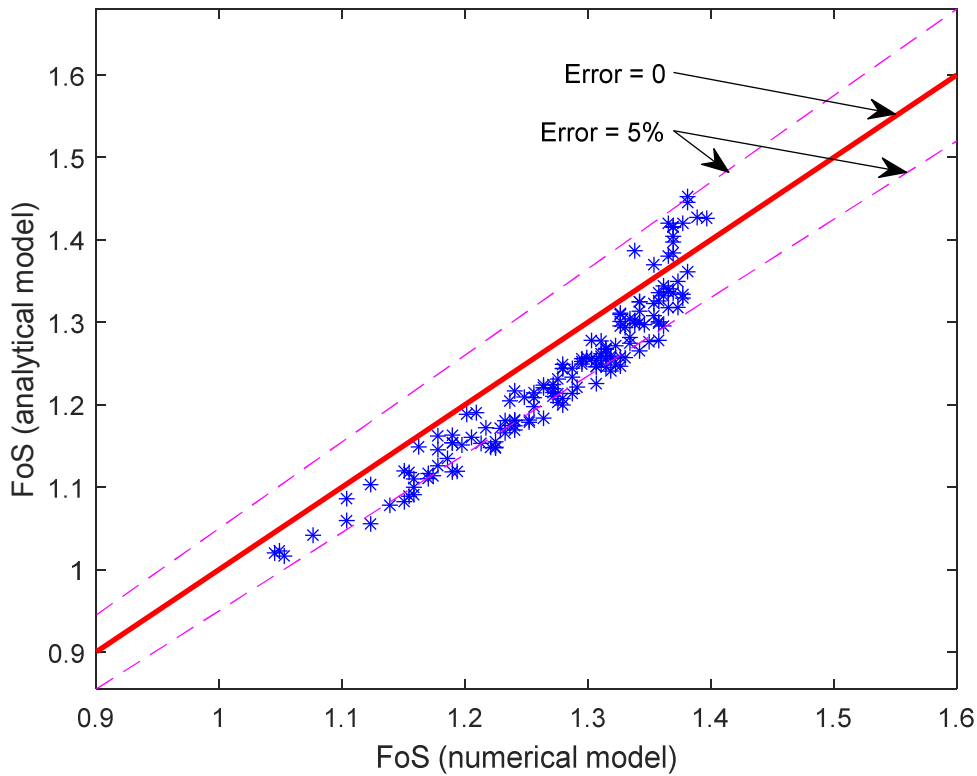
Figure 9. Comparison of the FoS values for 150 sets of input parameters

Using the analytical model, rather than the numerical one, can reduce the computational time of a stability analysis for the studied dam from 20 minutes to 10 seconds in an Intel Xeon CPU E5-1620 3.5 GHz PC. Such a reduction in computational time is very significant for a reliability analysis which needs usually a large number of calls to a deterministic model. Given that the analytical model can give reasonable FoS values compared to the numerical one but with a reduced time, the following analyses are all based on the analytical model.

5 Reliability analysis results by the reference method MCS

This section presents the reliability analysis for the studied dam using the reference method MCS. The uncertainties in the soil properties C', ϕ' and γ_d are quantified using random fields or random variables with the parameters presented in the sections

509 3.2 and 3.3. In addition, the effect of autocorrelation distances on the dam failure

510 probability is discussed.

511 **5.1 Reliability analysis results**

512 20 000 deterministic calculations are performed in the reliability analysis by an MCS

513 with the Latin Hypercube sampling technique. For each calculation, 2 110

514 independent standard random variables ξ_i are generated firstly. The first two ξ_i are

515 transformed to physical values of C' using the iso-probabilistic method with the

516 specific PDF presented in Table 1. The rest ξ_i are used in the K-L expansion for the

517 generation of the three random fields of γ_d. The three random fields of ϕ' are then

518 obtained by a transformation from those of γ_d using the Caquot's relation.

519

520 Figure 10 shows the PDF of the obtained 20 000 FoS values for the two distribution

521 types, and Table 3 gives the reliability results.
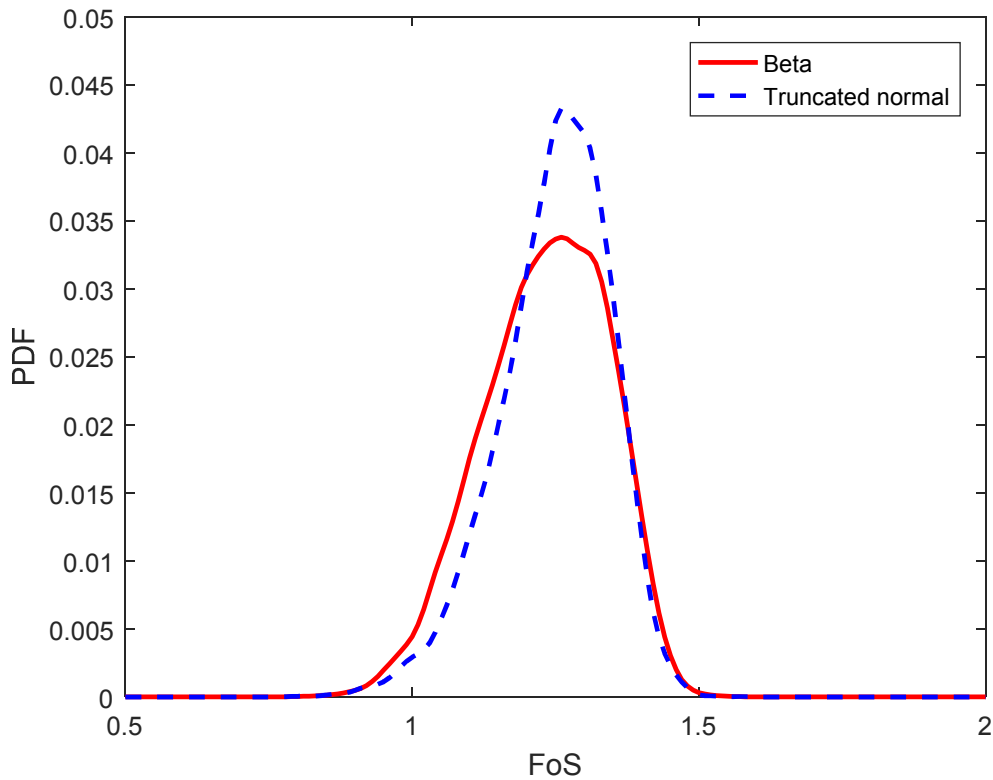
522

523 **Figure 10. PDF of the FoS values obtained by the MCS with two distributions**

Table 3. Reliability results obtained by the MCS with two distributions

Distribution	Failure probability			Statistical moments of FoS	
	Pf_{direct}	Pf_{con}	CoV_{Pf}	Mean	Standard deviation
Beta	0.022	4.4×10^{-6}	4.71%	1.232	0.108
Truncated normal	0.016	3.2×10^{-6}	5.61%	1.248	0.097

525

526　From Figure 10, it can be observed that the PDF curve obtained by the truncated

527　normal distribution (PDF_N) is taller and narrower than the one of beta distribution

528　(PDF_B). It means that the FoS values are less dispersive if a truncated normal

529　distribution is assumed for the input random variables. More precisely, the two PDF

530　curves are almost superposed for relative high FoS values (bigger than 1.4), while the

531　PDF_N is significantly lower than the PDF_B for relative small FoS values (smaller than

532　1.2). This is because of the probability of generating a small value of C' in the Shell

533　zone drawn from the fitted beta distribution is higher than the truncated normal

534　distribution, as presented in Figure 4. In addition, the two curves are not symmetric.

535　They are considered to be negatively skewed with a relatively bigger tail at the left. It

536　can be explained by the fact that the distribution of the input variables is not

537　symmetric and that some variables have more small values, such as C' in the Shell

538　zone as shown in Figure 4.

539

540　The direct failure probability Pf_{direct} of the dam under a pseudo-static acceleration of

541　2.4 m.s^{-2} is estimated to be equal to 0.022 and 0.016 respectively by the two

542　distributions. These values are then multiplied by a coefficient of 1/5000 to consider

543　the seismic occurrence probability and become equal to 4.4×10^{-6} and 3.2×10^{-6}

544　respectively. As for the statistical moments of the FoS values, the beta assumption

545　gives a slightly lower value for the mean but a bigger value for the standard deviation,

546 compared to the truncated normal assumption. A big value of standard deviation

547 means a high level of data scatter. This is consistent with the observation in Figure 10.

548

549 In conclusion, the dam failure probability under a pseudo-static loading condition is

550 estimated to be around 4×10^{-6}. The two distribution assumptions lead to similar

551 results with the same order of magnitude. The beta distribution gives slightly more

552 conservative results in term of the failure probability. As the beta distribution

553 describes better the variability of the soil properties as shown in Figure 4 and is

554 conservative in the design, this type of distribution is adopted for the next analyses.

555 **5.2 Influence of the autocorrelation distance**

556 One of the factors which can influence reliability results is autocorrelation distance. It

557 defines by means of an autocorrelation function, the autocorrelation structure of a

558 random field. According to a literature review given by El-Ramly et al. [47], the

559 autocorrelation distance for soils is usually within a range of 10-40 m in the horizontal

560 direction, while it ranges between 1 and 3 m in the vertical direction. It is found that

561 the L_x and L_y in the Shell-1 zone (Table 2) are bigger than the values indicated in [47]

562 while the L_x in the Shell-2 zone is smaller than expected values. Therefore, careful

563 attention must be done to these parameters and their induced influence on the

564 reliability analysis.

565

566 Finally, the impact investigation is focused on the value of L_x in the Shell-2 zone

567 while the estimated autocorrelation distances in the Shell-1 zone are accepted for the

568 values in Table 2. The reasons are as follows: 1) the obtained large values of L_x and

569 L_y are expected for the Shell-1 zone since the materials are better selected and more

570 attention are given to its construction; 2) the upstream part of the backfill

571 embankment is considered to have a very limited influence on the dam stability under

572 steady state flow conditions; 3) large values of autocorrelation distances may lead to

573 bigger failure probabilities, so conservative designs as pointed in [13,48,49].

574

575 For the L_x value in the Shell-2 zone, a first improvement is made by fitting the

576 experimental semivariogram with other theoretical variogram models such as the

577 Gaussian and the spherical models [50]. The L_x is estimated to be equal to 6.7m for

578 the Gaussian model, and to 4.7m for the spherical model. These values are both

579 different to the one estimated with the exponential model (4.9m) as shown in the

580 section 3.3, and these differences may induce an impact on the dam failure

581 probability.

582

583 In order to quantify the influence induced by different values of L_x, a parametric

584 study is conducted. Several values of L_x in the Shell-2 zone are tested using the MCS.

585 The objective is to investigate the evolution of the dam failure probability with the L_x

586 value. For the sake of simplicity and clarity, the other values of autocorrelation

587 distance are rounded to integer values (see details in Table 4). In addition, the L_x

588 value in the Core zone is also varied. Totally, four cases are selected for the

589 parametric study. The L_x value in the Core and Shell-2 zones are decreased from 80 to

590 10m. These four cases allow investigating the influence of the horizontal

591 autocorrelation distance in the Core and Shell-2 zones on the dam failure probability.

592 The reference case in Table 4 refers to the values estimated by the variogram analysis

593 with the exponential model (see Table 2).

594 **Table 4. Selected values of L_x and L_y for the parametric study**

	Shell-1		Core		Shell-2	
	L_x (m)	L_y (m)	L_x (m)	L_y (m)	L_x (m)	L_y (m)
Case1	80	8	80	2	80	2
Case2	80	8	40	2	40	2
Case3	80	8	20	2	20	2

Case4	80	8	10	2	10	2
Reference case	78.1	7.8	13	1.5	4.9	1.9

596 By adopting different values of autocorrelation distance as shown in Table 4, four

597 complementary MCSs are performed. Figure 11 plots the four obtained failure

598 probabilities together with the one of the reference case. The first two moments of the

599 dam FoS for each case are also given in Figure 11.
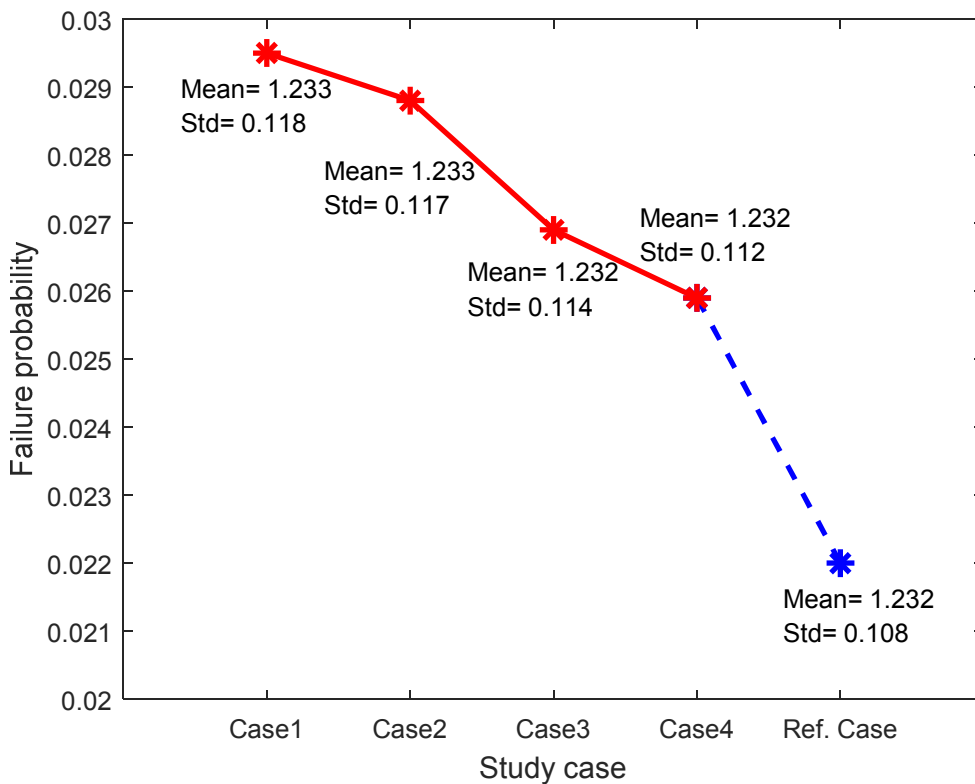
Figure 11. Influence of the L_x on the dam failure probability

602 It can be observed from Figure 11 that the horizontal autocorrelation distance in the

603 Core and Shell-2 zones have an influence on the dam failure probability. As the L_x

604 decreases, the Pf decreases. For example, a decrease of L_x from 80 to 10 m results in

605 a reduction of about 10% for the Pf (from 0.0295 to 0.0259). This finding has already

606 been confirmed by many researchers for different geotechnical engineering

607 [13,48,49]. Concerning the statistical moments, the mean value remains almost

608 constant whereas the standard deviation increases when increasing the L_x. This
609 indicates that the L_x has no impact on the mean value of the dam FoSs, whereas it
610 affects the FoSs dispersion of the dam. The reference case corresponds to the lowest
611 failure probability and the smallest standard deviation.

6 A comparative study of different reliability methods

613 This section presents the results and the relating interpretation of the comparative
614 study of the four selected approximated reliability methods. The objective is to
615 evaluate the performance of the considered methods for very high dimensional
616 stochastic problems.

617

618 The parametric study on the autocorrelation distance (presented in section 5.2) is re-
619 performed by the four reliability methods (SS, MM, SPCE/GSA and SPCE/SIR)
620 which are mentioned in the section Introduction and presented in section 2.3. The
621 obtained results in term of the failure probability for each case are plotted in Figure
622 12, and the numbers of calls to the deterministic model (N_{call}) for each case are
623 summarized in Table 5. Additionally, the results of the MCS are also provided and
624 considered as a standard reference for the comparison. In Table 5, the number of
625 required random variables ($N_{RV} = N_{RV\_KL} + 2$) for representing C', ϕ' and γ_d by
626 means of random fields or random variables is given as well. The N_{RV_KL} is the
627 number of random variables needed for generating relatively accurate random fields
628 of γ_d by using the K-L expansion method, and the number 2 represents the two
629 random variables of C' in the Shell and the Core zones. The information in Table 5
630 helps to visualize the effiency of each method by comparing the N_{RV} with the N_{call}.
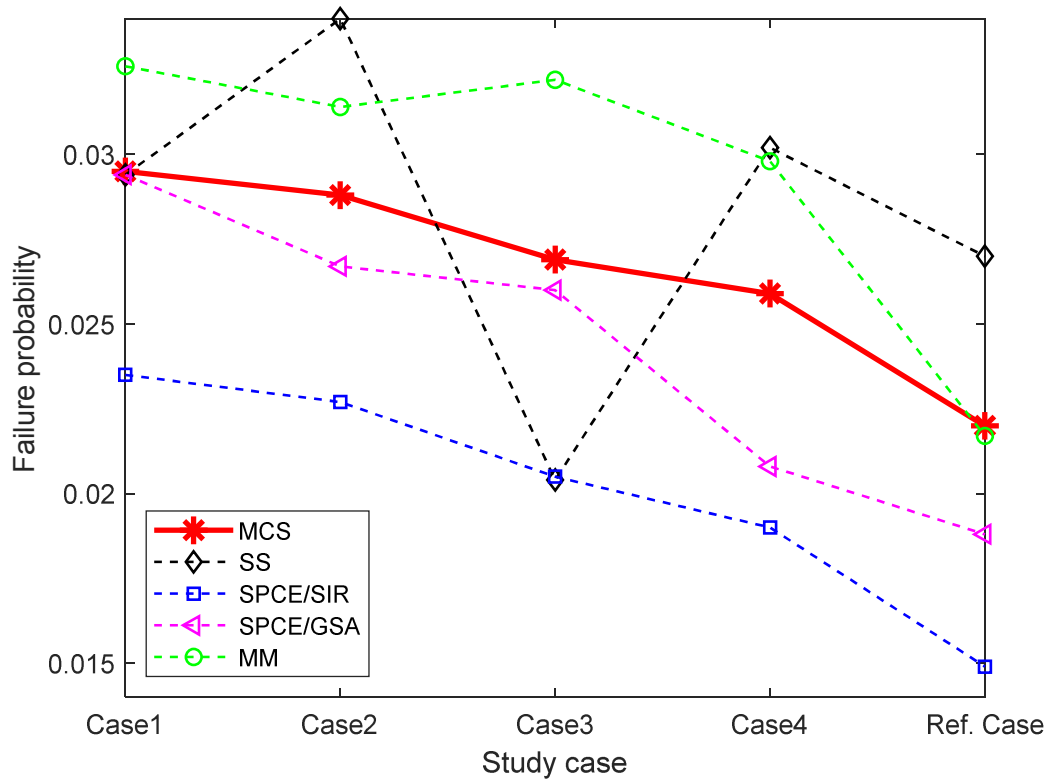
Figure 12. Comparison of the failure probability obtained by the five reliability methods

Table 5. Comparison of the necessary run numbers of the deterministic model for the five reliability methods

	Case 1	Case 2	Case 3	Case 4	Reference case
N_{RV}[1]	225	370	647	1207	2110
MCS	20000	20000	20000	20000	20000
SS	600	600	600	600	600
SPCE/SIR	1000	5000	8000	10000	15000
SPCE/GSA	3000	5000	8000	13000	18000
MM	1946	1755	2081	2026	1981

Note: [1]Number of required random variables for representing C', ϕ' and γ_d by means of random fields or random variables for each case

638   A quick review of Figure 12 reveals that the four methods can all give relatively

639   accurate failure probabilities compared to the results of MCS. The values of Pf are

640   within a same order of magnitude for different methods. For example, the Pf varies

641   between 0.015 and 0.027 for the Reference case according to the four methods.

642

643   Concerning the efficiency comparison presented in Table 5, it is found that all the

644   approximated methods need fewer calls of the deterministic model than the MCS.

645   This is the reason why these methods are an alternative to the MCS for reliability

646   analyses. Besides, the value of N_{RV} increased from Case1 to Case4, and the N_{RV} of the

647   Reference Case is the biggest one. This is because the autocorrelation distance L_x

648   value in the Core and Shell-2 zones are decreased from 80 to 10m. Smaller value of

649   the autocorrelation distance means that it needs more random variables N_{RV_KL} to

650   represent a random field with a specific error variance. By comparing the N_{RV} with

651   the N_{call} of each method, it is observed that the N_{call} of the methods MCS, SS and

652   MM is almost changeless to the N_{RV}. In other words, the efficiency of these three

653   methods is not related to the number of input random variables, but depends on, in

654   fact, the value of the target failure probability. However, the N_{call} of the two meta-

655   modelling methods (SPCE/GSA and SPCE/SIR) increases rapidly with increasing the

656   N_{RV}. This indicates that the efficiency of the meta-modelling method depends strongly

657   on the number of input random variables. Indeed, more input variables means that

658   more information is needed. Thus, a higher N_{call} will be required for constructing a

659   meta-model which will be used to replace an original mechanical model.

660

661   The following subsections give a detailed interpretation of the comparative study for

662   each reliability method. In the end, some concluding remarks of the comparative

663   study are summarised.

664   **6.1 The SS**

665 This method is the most efficient one, according to Table 5, which requires only 600

666 calls of the deterministic model. The N_{call} of the SS is much less than the MCS one

667 (about 3%) and is constant with the N_{RV} variation. This finding is not surprising since

668 the target failure probability is relatively high (around 0.022) and changes slightly

669 between the different proposed cases in the present problem. If a conditional

670 probability P_c of 0.2 is adopted for each simulation level, only 3 simulation levels are

671 needed to reach the final failure domain. In this study, the P_c is set to 0.2 and the

672 sample numbers in each simulation level (N_{level}) is set to 200. However, it is found

673 that the SS cannot produce a consistent evolution of Pf with L_x. The obtained values

674 of Pf are fluctuated from the Case 1 to the Reference case, while they are expected to

675 be monotone decreasing as shown by the MCS. This limitation originates from the

676 generation of the conditional samples in the SS. As a large number of random

677 variables are considered and more importantly those used for random field generation

678 have no physical meanings, it is thus very difficult to generate effective conditional

679 samples. This results in a large number of repeated samples in the SS. Given that the

680 number of these repeated samples is not constant (i.e. random) for each SS, the

681 obtained results are thus not steady.

682 **6.2 The SPCE/SIR**

683 According to Figure 12, this method gives always lower failure probability than the

684 MCS. This can be explained by the fact that a dimension reduction technique is

685 employed. As the dimension is reduced, the variability of the input parameters is

686 reduced. The estimated failure probability is thus smaller. Compared to the SS, this

687 method has a better performance in the parametric study i.e. the obtained values show

688 a clear reduction trend of Pf with decreasing L_x. Concerning the efficiency, the N_{call}

689 is found not constant for different cases but increases from the Case 1 to the

690 Reference case. The N_{call} for the Reference case is even very close to the MCS one.

691 An explanation is given as follows. The required number of input random variables

692   for the random field generation increased since the L_x becomes smaller. Therefore,

693   the construction of a meta-model needs more training points i.e. more deterministic

694   simulation. As a result, it is not recommended to use this method if the N_{RV} is large

695   (e.g. >2500) from a point of view of efficiency.

6.3 The SPCE/GSA

697   This method is the most accurate one based on Figure 12. The obtained values of Pf

698   are extremely close to the ones of the MCS. Except to this remark, similar

699   observations to the SPCE/SIR can also be noted: 1) the estimated values of Pf are all

700   lower than those of the MCS; 2) the parametric study can be correctly conducted; 3)

701   the N_{call} increases with decreasing the L_x and the N_{call} for the Reference case is even

702   very close to the one of the MCS. The interpretation to these observations given above

703   remains valid as well for this method. In addition, it is found that this method is

704   always less efficient than the SPCE/SIR. This difference originates from the different

705   dimension reduction techniques employed in the two methods. For the SPCE/GSA, it

706   should always construct a 2-order meta-model with a full dimension. On the contrary,

707   the dimension is reduced before constructing meta-models in the SPCE/SIR. For very

708   high dimensional stochastic problems, considerable deterministic simulations are

709   required even for constructing a 2-order SPCE meta-model.

6.4 The MM

711   This method is the second efficient one according to Table 5 and it shows also a good

712   performance in estimating the value of Pf. Given its simplicity and easy

713   implementation procedure, it is a good alternative to the MCS for such a very high

714   dimensional stochastic problem. However, this article only evaluates the MM for the

715   cases of relative high failure probability. Careful attention should be paid when

716   applying this method to calculate low failure probabilities since it may lead to large

717   errors as pointed out in [33]. Besides, this method is not able to carry out a parametric

718   study of L_x as expected since the obtained Pf results fluctuate. Theoretically, the

719   collection of all the moments (of all orders, from 0 to ∞) uniquely describes a

720   bounded distribution. Then, failure probabilities can be determined by estimating the

721   tail area of the distribution. In the present study, only four moments are collected and

722   the tail area is estimated by an approximated way (Eq. 8 and 9). The induced errors

723   are not related to the N_{RV} or L_x of the problem but depend on the complexity of the

724   FoS distribution and the target value of the dam failure probability (tail area). It may

725   lead to a large error for a lower Pf but a small error for a higher Pf. As a result, the

726   obtained Pf values in the parametric study are not monotonously decreasing.

727   **6.5 Concluding remarks**

728   Here gives a summary of the remarks observed in Figure 12 and Table 5.

729   a) The most accurate method is the SPCE/GSA and the most efficient one is the SS.

730   b) The efficiency of the two meta-modelling methods strongly depends on the

731   number of input variables, while the N_{call} of the sampling-based methods (the SS

732   and the MM) is related to the target value Pf. As the Pf doesn't vary significantly

733   from Case1 to the Reference Case, the N_{call} of SS and MM is more or less

734   changeless.

735   c) The sampling-based methods cannot produce a consistent evolution of Pf in the

736   parametric study of the L_x whereas the meta-modelling methods perform well in

737   such a study.

738   d) The sampling-based methods are more efficient than the two considered meta-

739   modelling methods for very high dimensional stochastic problems.

740   e) The two meta-modelling methods estimate smaller values of Pf compared to the

741   MCS. This is because that dimension reduction techniques are employed in these

742   two methods.

743

744   It should be noted that the conducted comparative study is related to a case of a

745   relatively high failure probability (order of 10^{-2}). The performance of the four

746 methods for estimating low failure probabilities (e.g. $<10^{-4}$) in the context of very

747 high dimensional stochastic problems is not investigated and thus unknown. This is a

748 difficult issue in the field of reliability analyses to assess an approximated method for

749 very low Pf, since the consuming time of running an MCS is very high even with a

750 simplified deterministic model. The present study provides first insights into the

751 performance of the four reliability methods in the context of very high stochastic

752 problems, and some concluding remarks (e.g. the points b, c and e mentioned above)

753 can be extended to the cases of low Pf.

7 Conclusions and perspectives

755 In this article, a probabilistic stability analysis of an earth dam is presented. The

756 uncertainties in three soil properties (C', ϕ' and γ_d) are considered in the analysis and

757 quantified by exploiting the project-specific data. A large number of available geo-

758 localized γ_d measurements allow accounting for the soil spatial variability by

759 estimating the autocorrelation structure with a variogram analysis. The MCS is

760 adopted for performing the reliability analysis. Two distribution types for the input

761 random variables are considered and compared in the article. Besides, the effect of the

762 L_x on the dam Pf is investigated. Such a study is original because it uses real dam

763 construction data, proposes using the benefits of geostatistics (a very high

764 dimensional stochastic problem) and presents a procedure on how to produce

765 meaningful statistical estimations of soil variability with limited measurements. This

766 study can then be used as a part of a global dam safety assessment combined with a

767 risk analysis as reported in [51].

768

769 By benefiting to the results of the deterministic simulations collected in the performed

770 MCS, a comparative study is carried out. It aims at evaluating the performance of

771 different reliability methods for very high dimensional stochastic problems. Both the

772 accuracy and efficiency are considered in the comparison. The results show that the

773 most accurate method is the SPCE/GSA and the most efficient method is the SS. The

774 efficiency of the methods SS and MM are independent to the number of input

775 variables while the necessary N_{call} of the methods SPCE/GSA and SPCE/SIR can be

776 very important (close to the N_{call} of an MCS) when a large number of random

777 variables are involved. For a first order estimate, the methods SS and MM are

778 sufficient to give relatively accurate results. Nevertheless, it should be noted that these

779 two methods were not sufficiently accurate for the parametric study of L_x since the

780 obtained values of Pf fluctuate.

781

782 This study also has some weakness points which will allow possible improvements

783 for future works:

784   - It is commonly recognized that a negative correlation exists between C' and ϕ'

785   [42]. However, no correlation is considered in this study for the two soil

786   properties due to the limited number of available triaxial test results and the

787   employed method [5] for generating the values of C' and ϕ'.

788   - The C' is represented by means of random variables. Its spatial variability is

789   thus ignored in the present study,

790   - For the sake of simplicity and consistency with other studies, only stationary

791   unconditional random fields are considered in this article. The effects of more

792   complex random fields (non-stationary or conditional) could be investigated in

793   future studies,

794   - The performance of the four reliability methods is only assessed for the cases

795   of relatively high failure probability. For the cases with low Pf, the accuracy

796   and efficiency of the four methods remain unknown for very high dimensional

797   stochastic problems.

798 # 8 List of symbols

Soil properties

γ_d (g/cm^3)	Dry density
C' (kPa)	Effective cohesion
ϕ' (^{o})	Friction angle

Some important symbols used in the statistical models

μ	Mean value
σ	Standard deviation
S	Truncation term of the PCE series expansion
L_x and L_y	Horizontal and vertical autocorrelation distance
N_{MCS}	Number of MCS population
G	Performance function
β	Reliability index
Pf	Probability of Failure
a and b	Beta distribution parameters
ξ	A vector of standard uncorrelated random variable
N_{RV}	Number of random variables
N_{call}	Number of calls to the deterministic model

Abbreviation

MCS	Monte Carlo simulation
SS	Subset Simulation
MM	Moment method
SPCE	Sparse Polynomial Chaos Expansions
GSA	Global Sensitivity Analysis
SIR	Sliced Inverse Regression
FoS	Factor of Safety
CoV	Coefficient of variation
PDF	Probability Density Function
K-L	Karhunen–Loève expansions

799

9 Acknowledgement

10 References

[1] Liang RY, Nusier OK, Malkawi AH. A reliability based approach for evaluating the slope stability of embankment dams. Eng Geol 1999;54:271–85. doi:10.1016/S0013-7952(99)00017-4.

[2] Gaouar M, Fogli M, Bacconnet C. Reliability of earth dams: an approach based on random fields models. Int. Conf. Appl. Stat. Probab. Civ. Eng., Sydney: 2000, p. 355–61.

[3] Babu GS, Srivastava A. Reliability Analysis of Earth Dams. J Geotech Geoenvironmental Eng 2010;136:995–8. doi:10.1061/(ASCE)GT.1943-5606.0000313.

[4] Yi P, Liu J, Xu C. Reliability Analysis of High Rockfill Dam Stability. Math Probl Eng 2015;2015. doi:10.1155/2015/512648.

[5] Mouyeaux A, Carvajal C, Bressolette P, Peyras L, Breul P, Bacconnet C. Probabilistic stability analysis of an earth dam by Stochastic Finite Element Method based on field data. Comput Geotech 2018;101:34–47. doi:10.1016/j.compgeo.2018.04.017.

[6] Dawson EM, Roth WH, Drescher A. Slope stability analysis by strength reduction. Géotechnique 1999;49:835–40. doi:10.1680/geot.1999.49.6.835.

[7] Rubinstein RY. Simulation and the Monte Carlo Method. New York: John Wiley & Sons Ltd; 1981.

[8] Sudret B, Der Kiureghian A. Stochastic finite element methods and reliability. A state-of-the-art-report. University of California, 2000.

[9] Au S-K, Beck JL. Estimation of small failure probabilities in high dimensions by subset simulation. Probabilistic Eng Mech 2001;16:263–77. doi:10.1016/S0266-8920(01)00019-4.

828   [10]   Ahmed A, Soubra A. Application of the subset simulation approach to spatially

829   varying soils. In: Phoon K-K, Ching J, editors. Risk Reliab. Geotech. Eng.,

830   CRC Press; 2014, p. 561–77.

831   [11]   Rosenblueth E. Point estimates for probability moments. Proc Natl Acad Sci

832   1975;72:3812–4. doi:10.1073/pnas.72.10.3812.

833   [12]   Mollon G, Dias D, Soubra A-H. Probabilistic Analysis of Circular Tunnels in

834   Homogeneous Soil Using Response Surface Methodology. J Geotech

835   Geoenvironmental Eng 2009;135:1314–25. doi:10.1061/(ASCE)GT.1943-

836   5606.0000060.

837   [13]   Pan Q, Dias D. Probabilistic evaluation of tunnel face stability in spatially

838   random soils using sparse polynomial chaos expansion with global sensitivity

839   analysis. Acta Geotech 2017;12:1415–29. doi:10.1007/s11440-017-0541-5.

840   [14]   Sudret B, Marelli S, Wiart J. Surrogate models for uncertainty quantification:

841   An overview. 2017 11th Eur. Conf. Antennas Propag., IEEE; 2017, p. 793–7.

842   doi:10.23919/EuCAP.2017.7928679.

843   [15]   Hurtado J, Alvarez D. Neural-network-based reliability analysis: a comparative

844   study. Comput Methods Appl Mech Eng 2001;191:113–32.

845   doi:10.1016/S0045-7825(01)00248-1.

846   [16]   Schueremans L, Van Gemert D. Benefit of splines and neural networks in

847   simulation based structural reliability analysis. Struct Saf 2005;27:246–61.

848   doi:10.1016/j.strusafe.2004.11.001.

849   [17]   Kaymaz I. Application of kriging method to structural reliability problems.

850   Struct Saf 2005;27:133–51. doi:10.1016/j.strusafe.2004.09.001.

851   [18]   Echard B, Gayton N, Lemaire M. AK-MCS: an active learning reliability

852   method combining Kriging and Monte Carlo simulation. Struct Saf

853   2011;33:145–54. doi:10.1016/j.strusafe.2011.01.002.

854   [19]   Li TZ, Yang XL. An efficient uniform design for Kriging-based response

855   surface method and its application. Comput Geotech 2019;109:12–22.

856   doi:10.1016/j.compgeo.2019.01.009.

[20]   Sudret B. Polynomial Chaos Expansions and Stochastic Finite Element
       Methods. In: Phoon K-K, Ching J, editors. Risk Reliab. Geotech. Eng., CRC
       Press; 2014, p. 265–300.

[21]   Blatman G, Sudret B. Adaptive sparse polynomial chaos expansion based on
       least   angle   regression.   J   Comput   Phys   2011;230:2345–67.
       doi:10.1016/j.jcp.2010.12.021.

[22]   Al-bittar T, Soubra A-H. Efficient sparse polynomial chaos expansion
       methodology for the probabilistic analysis of computationally-expensive
       deterministic models. Int J Numer Anal Methods Geomech 2014;38:1211–30.
       doi:10.1002/nag.2251.

[23]   Pan Q, Dias D. Sliced inverse regression-based sparse polynomial chaos
       expansions for reliability analysis in high dimensions. Reliab Eng Syst Saf
       2017;167:484–93. doi:10.1016/j.ress.2017.06.026.

[24]   Guo X, Dias D, Carvajal C, Peyras L, Breul P. Reliability analysis of
       embankment dam sliding stability using the sparse polynomial chaos
       expansion. Eng Struct 2018;174:295–307. doi:10.1016/j.engstruct.2018.07.053.

[25]   Baecher GB, Christian JT. Reliability and Statistics in Geotechnical
       Engineering. John Wiley & Sons; 2005. doi:10.1198/tech.2005.s838.

[26]   Phoon KK. Numerical recipes for reliability analysis – a primer. In: Phoon K-
       K, Ching J, editors. Reliab. Des. Geotech. Eng., CRC Press; 2008, p. 545.

[27]   Li C-C, Der Kiureghian A. Optimal discretization of random fields. J Eng
       Mech 1993;119:1136–54. doi:10.1061/(ASCE)0733-9399(1993)119:6(1136).

[28]   Cho SE, Park HC. Effect of spatial variability of cross-correlated soil properties
       on bearing capacity of strip footing. Int J Numer Anal Methods Geomech
       2010;34:1–26. doi:10.1002/nag.791.

[29]   Li D, Chen Y, Lu W, Zhou C. Stochastic response surface method for
       reliability analysis of rock slopes involving correlated non-normal variables.

884   Comput Geotech 2011;38:58–68. doi:10.1016/j.compgeo.2010.10.006.

885   [30] Wang Y, Cao Z, Au SK. Efficient Monte Carlo Simulation of parameter
886   sensitivity in probabilistic slope stability analysis. Comput Geotech
887   2010;37:1015–22. doi:10.1016/j.compgeo.2010.08.010.

888   [31] Li HS, Cao ZJ. Matlab codes of Subset Simulation for reliability analysis and
889   structural optimization. Struct Multidiscip Optim 2016;54:391–410.
890   doi:10.1007/s00158-016-1414-5.

891   [32] Zhao YG, Ono T. Moment methods for structural reliability. Struct Saf
892   2001;23:47–75. doi:10.1016/S0167-4730(00)00027-8.

893   [33] Napa-García GF, Beck AT, Celestino TB. Reliability analyses of underground
894   openings with the point estimate method. Tunn Undergr Sp Technol
895   2017;64:154–63. doi:10.1016/j.tust.2016.12.010.

896   [34] Sudret B. Global sensitivity analysis using polynomial chaos expansions.
897   Reliab Eng Syst Saf 2008;93:964–79. doi:10.1016/j.ress.2007.04.002.

898   [35] Blatman G, Sudret B. Sparse polynomial chaos expansions and adaptive
899   stochastic finite elements using a regression approach. Comptes Rendus
900   Mécanique 2008;336:518–23. doi:10.1016/j.crme.2008.02.013.

901   [36] Blatman G, Sudret B. An adaptive algorithm to build up sparse polynomial
902   chaos expansions for stochastic finite element analysis. Probabilistic Eng Mech
903   2010;25:183–97. doi:10.1016/j.probengmech.2009.10.003.

904   [37] LI KC. High dimensional data analysis via the SIR/PHD approach. 2000.

905   [38] Guo X, Baroth J, Dias D, Simon A. An analytical model for the monitoring of
906   pore water pressure inside embankment dams. Eng Struct 2018;160:356–65.
907   doi:10.1016/j.engstruct.2018.01.054.

908   [39] Phoon K-K, Kulhawy FH. Characterization of geotechnical variability. Can
909   Geotech J 1999;36:612–24. doi:10.1139/t99-038.

910   [40] StructX. Density Ranges for Different Soil Types 2015.
911   http://structx.com/Soil_Properties_002.html (accessed October 24, 2017).

912   [41]   Jiang S-H, Li D-Q, Zhang L-M, Zhou C-B. Slope reliability analysis
913   considering spatially variable shear strength parameters using a non-intrusive
914   stochastic   finite   element   method.   Eng   Geol   2014;168:120–8.
915   doi:10.1016/j.enggeo.2013.11.006.

916   [42]   Tang XS, Li DQ, Chen YF, Zhou CB, Zhang LM. Improved knowledge-based
917   clustered partitioning approach and its application to slope reliability analysis.
918   Comput Geotech 2012;45:34–43. doi:10.1016/j.compgeo.2012.05.001.

919   [43]   Lumb P. Safety factors and the probability distribution of soil strength. Can
920   Geotech J 1970;7:225–42. doi:10.1139/t70-032.

921   [44]   Loudière D, Hoonakker M, Le Delliou P. Risque sismique et sécurité des
922   ouvrages hydrauliques. 2014.

923   [45]   Itasca. FLAC 7.0 reference manual. Minneapolis: 2011.

924   [46]   Li Y-C, Chen Y-M, Zhan TLT, Ling D-S, Cleall PJ. An efficient approach for
925   locating the critical slip surface in slope stability analyses using a real-coded
926   genetic algorithm. Can Geotech J 2010;47:806–20. doi:10.1139/T09-124.

927   [47]   El-Ramly H, Morgenstern NR, Cruden DM. Probabilistic stability analysis of a
928   tailings dyke on presheared clay-shale. Can Geotech J 2003;40:192–208.
929   doi:10.1139/t02-095.

930   [48]   Cho SE. Effects of spatial variability of soil properties on slope stability. Eng
931   Geol 2007;92:97–109. doi:10.1016/j.enggeo.2007.03.006.

932   [49]   Liu LL, Cheng YM, Zhang SH. Conditional random field reliability analysis of
933   a   cohesion-frictional   slope.   Comput   Geotech   2017;82:173–86.
934   doi:10.1016/j.compgeo.2016.10.014.

935   [50]   Fenton GA, Griffiths D V. Risk Assessment in Geotechnical Engineering.
936   Hoboken,   NJ,   USA: John   Wiley   &   Sons,   Inc.;   2008.
937   doi:10.1002/9780470284704.

938   [51]   Peyras L, Carvajal C, Felix H, Bacconnet C, Royet P, Becue J-P, et al.
939   Probability-based assessment of dam safety using combined risk analysis and

940   reliability methods – application to hazards studies. Eur J Environ Civ Eng

941   2012;16:795–817. doi:10.1080/19648189.2012.672200.

942